Publications of the Astronomical Society of the Pacific, 133:034502 (8pp), 2021 March https://doi.org/10.1088/1538-3873/abc8d9

Simulation Study of on Sky Performance of a New 20W Class Macro–Micro Pulse Laser for Sodium Laser Guide Star

Hong-Yang Li[1,2], Lu Feng[2], Jian-Li Wang[3,4], Jie Liu[3,4], Sui-Jian Xue[2], and Zhi-Xia Shen[2]
[1] University of Chinese Academy of Sciences, Beijing 100049, People's Republic of China; lihongyang@nao.cas.cn
[2] CAS Key Laboratory of Optical Astronomy, National Astronomical Observatories, Chinese Academy of Sciences, Beijing 100101, People's Republic of China
jacobfeng@bao.ac.cn
[3] Changchun Institute of Optics, Fine Mechanics and Physics, Chinese Academy of Sciences, Changchun 130033, People's Republic of China
[4] Key Laboratory of Space object and Debris Observation, Purple Mountain Observatory, Chinese Academy of Sciences, Nanjing, 210008, People's Republic of China
Received 2020 August 14; accepted 2020 November 9; published 2021 February 17

Abstract

As one crucial component for the latest generation of adaptive optics, tremendous efforts have been put into the development of high performance 20 W class sodium laser guide star laser system. Two such systems, the continuous wave laser by Toptica, and the quasi-continuous pulse laser by TIPC were extensively studied with simulation and field tests. A new type of 20 W class sodium laser, macro–micro pulse laser, is currently being developed by CIOMP. In this paper, we will study its on-sky performance with simulation based on Monte Carlo rate equation method. The predicted coupling efficiency for this laser in the zenith direction in Changchun is 179.73 photons s^{-1} W^{-1}/(atoms m^{-2}). The variation of coupling efficiency of this type of laser with pointing direction and the effect of D2b repumping are also studied and reported in this paper.

Unified Astronomy Thesaurus concepts: Astronomical instrumentation (799); Astronomical methods (1043); Astronomical techniques (1684); Laser guide stars (904)

1. Introduction

Adaptive Optics (AO) system helps large ground-based telescope alleviate degradation of image quality by atmospheric turbulence and thus achieve a near diffraction limited image quality (Hardy 1998). However, such a system requires a bright guide star as a reference source to detect the atmospheric turbulence in real time. Even for extremely large telescope with unparalleled light gathering capability, like the Thirty Meter Telescope, natural guide stars with sufficient brightness to close the AO loop only cover a fraction of the sky (Ellerbroek & Andersen 2008). It is therefore crucial to have artificial guide star that could be pointed to any direction in the sky which would vastly improve the sky coverage of AOs system. By projecting a 589.159 nm laser onto the sodium layer which is normally distributed at an altitude around 90–110 km, it is possible to produce backscattered photon that could be used as laser guide star (Max et al. 1994). This technique, the sodium laser guide star, became very popular in recent year. However, due to the physics of sodium atoms, many parameters of the laser and environment would hinder the efficiency for the generation of the backscattered photons. It is therefore necessary to explore the optimum parameters for certain types of sodium lasers with constraints either from environments and practical considerations and field tested in the astronomical community for astronomical applications.

To date, especially in the past decade, based on published papers, two types of 20 W class sodium lasers have been actively developed, studied and field tested in the astronomical community. One of them is a Raman fiber frequency doubling Continuous Wave (CW) sodium laser that has already been commissioned at ESO's Very Large Telescope and Keck Observatory (Calia et al. 2010, 2014; Chin et al. 2016). The other is a solid-state Quasi-continuous Wave (QCW) 100 μs pulsed sodium laser developed by Technical Institute of Physics and Chemistry, Chinese Academy of Sciences (TIPC) (Wang et al. 2014; Bian et al. 2016a, 2016b, 2017, 2020; Xu et al. 2017). Although this laser hasn't been commissioned for operation yet, field tests and simulation results (Jin et al. 2014; Feng et al. 2016; Otarola et al. 2016) showed similar on-sky brightness performance as the Raman fiber CW laser.

Changchun Institute of Optics, Fine Mechanics and Physics, Chinese Academy of Sciences (CIOMP) is currently developing a new 20 W class sodium laser for astronomical AOs system. The laser utilizes a temporal format called macro–micro pulse format, which is much different from the other two aforementioned lasers. This type laser was first proposed in 1990s and a lot of theoretical studies were done later (Jeys 1991; Bradley 1992; Milonni et al. 1998; Telle et al. 1998). Then, Kibblewhite et al. (1998) designed and built a 8W sum frequency laser and carried out field test on the NOAO Vacuum Telescope Tower at Sac Peak. The new laser of CIOMP has larger power and the macro micro pulse format contains "macro" pulses that last $\sim 160\,\mu$s for each pulse

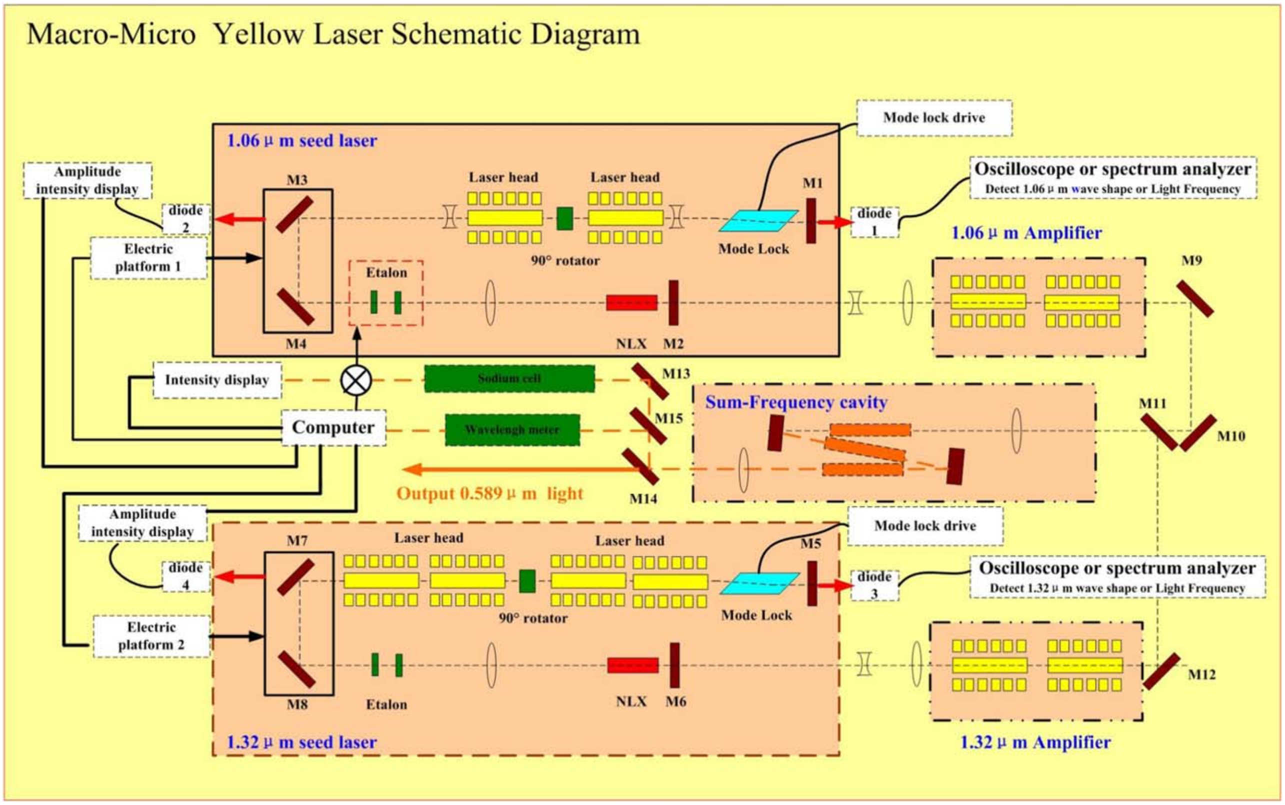

Figure 1. The schematic diagram of 589 nm macro–micro pulse laser.

running with a repetition frequency of 500 Hz. Within each of these "macro" pulse envelopes, there are thousands of very short nano-seconds "micro" pulses repeating at a frequency of 100 MHz. Macro–micro pulse format of this laser combined with range gating could easily eliminate contamination from Rayleigh backscatter which could be annoying to remove especially for multi laser guide stars application scenario. The 10 ns interval of mode-locked micro pulse format is closer to the fluorescence lifetime 16 ns of sodium atom, which in theory might improve the excitation efficiency of sodium atoms comparing with quasi continuous wave laser because instantaneous power density is higher. Due to the design of this macro–micro format laser, the spectrum of this laser also differs from the other two lasers. Therefore, it would be interesting to simulate how it would perform on-sky, to answer whether it would reach a similar performance as the other two lasers in the early phase of the development, and this is the purpose of the work described in this paper.

In this paper, the CIOMP macro–micro pulse laser will be presented in Section 2 and we will described the parameters relating to simulation and our simulation tool more in detail in Section 3. Results of the simulation will be presented in Section 4. We will discuss what has been learned from these simulation results in Section 5.

2. The CIOMP Macro–Micro Pulse Laser

The schematic diagram of the CIOMP macro–micro pulse laser system is shown in Figure 1. The laser system mainly consists of three parts: a 1064 nm macro–micro pulse mode locked laser, a 1319 nm macro–micro pulse mode locked laser and a nonlinear sum-frequency cavity. Two side pumped amplifiers are used for amplification of the 1064 and 1319 nm seed lasers. Then the sum-frequency cavity combines the two beams and outputs a macro–micro pulse laser beam of 589 nm wavelength. A power attenuator which is used for changing the output power of the laser, and an electro-optic modulator (EOM) will be installed after M14. The purpose of the EOM is to modulate part of the laser output which is at sodium D2A line into sodium D2B line. The power ratio of the side frequency (D2B line) to the total laser power can be continuously adjusted by changing the modulation depth.

The center wavelength of the laser is aligned to 589.159 nm, D2A line. The wavelength of the laser is monitored by a wavelength meter (60 MHz accuracy), combined with a PID controller, the wavelength can be adjusted by controlling an etalon's angle as well as its temperature inside the 1064 nm laser's cavity. Furthermore, we also use a sodium cell and an oscilloscope to monitor the output laser to eliminate possible drift of the wavelength meter. The other main parameters of the

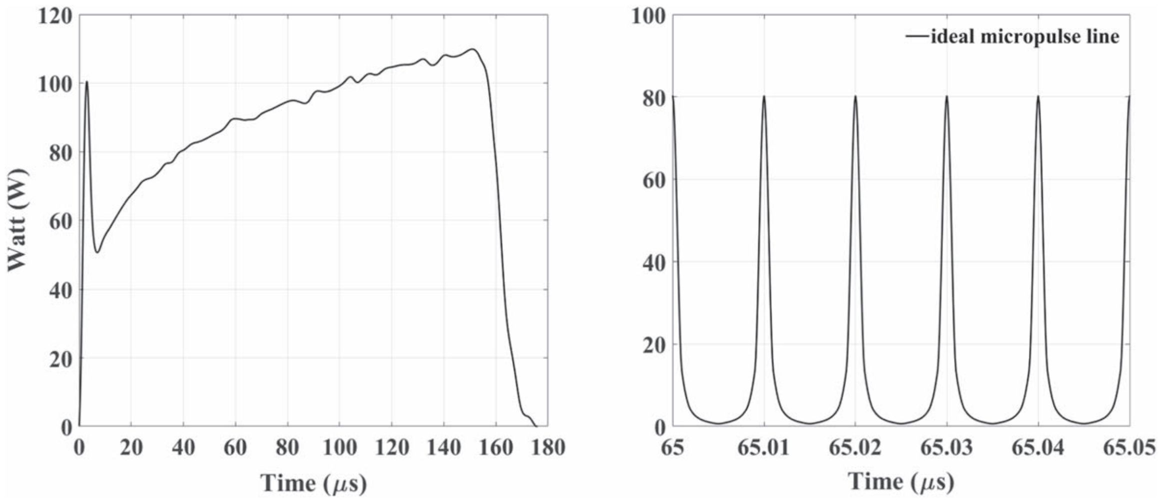

Figure 2. Temporal format of the laser output. (Left) The 160 μs macro pulse of the laser. (Right) Zoomed in a tiny portion of the macro pulse, one can see very narrow Lorentzian shaped micro pulses.

Table 1
Laser Parameters for CIOMP 20 Watt Macro–micro Pulse Sodium Laser

Parameter Name	Value
Center wavelength	589.159 nm
Linewidth	~0.5 GHz
Longitudinal mode interval	100 MHz
Longitudinal mode width (FWHM)	4 MHz
Macro pulse repetition rate	500 Hz
Macro pulse width	~ 160 μs
Micro pulse repetition rate	100 MHz
Micro pulse width	~900 ps
Average power	20 W
Beam quality	1.4
Divergence angle	1 mrad
Polarization	circular
D2b repumping factor	0%, 5%, 10%, 15%, 30%, 40%, 50%
Laser guide star on sky spot size (FWHM at 92 km)	1.″25

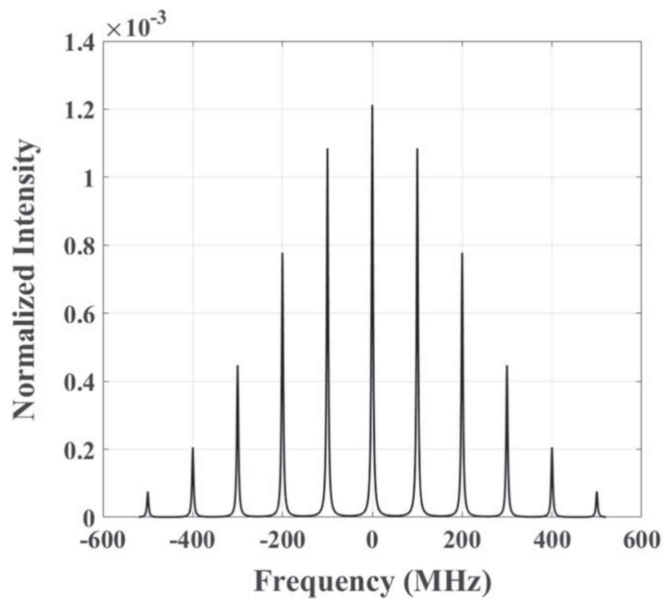

Figure 3. Spectral format of the laser. The interval between these Lorentzian shaped longitudinal modes is 100 MHz, and the width for each longitudinal modes is 4 MHz.

laser are summarized in Table 1. The temporal format of the laser is consisted of a series of "macro" pulses, each lasts about 160 μs with a repetition frequency of 500 Hz (Figure 2 (left)). Within each "macro" pulse envelope, there are thousands of "micro" pulses. These micro pulses have a repetition frequency of 100 MHz. The Full Width Half Maximum (FWHM) of the micro pulse is 900 pico-second (Figure 2 (right)).

The spectral format of the laser is shown in Figure 3. Several longitudinal modes are presented in the output spectrum. The distance between each longitudinal mode is 100 MHz. For each Lorentzian shaped mode, the FWHM of these modes are the same, which is 4 MHz.

The average output power is 20W, with a beam quality $M^2 = 1.4$. The polarization of the laser could be adjusted with a Quarter-wave Plate. The default polarization is circular unless devices that require linear polarization input, such as EOM, were used. In those cases, the QWP will be installed after the EOM to make sure the polarization of the laser before launch is still circular. The projected on-sky laser guide starspot size is expected to be 1.″25 in Changchun.

3. Simulation

We used a simulation tool called Photon Return Simulation code (Feng et al. 2015) that we developed previously for

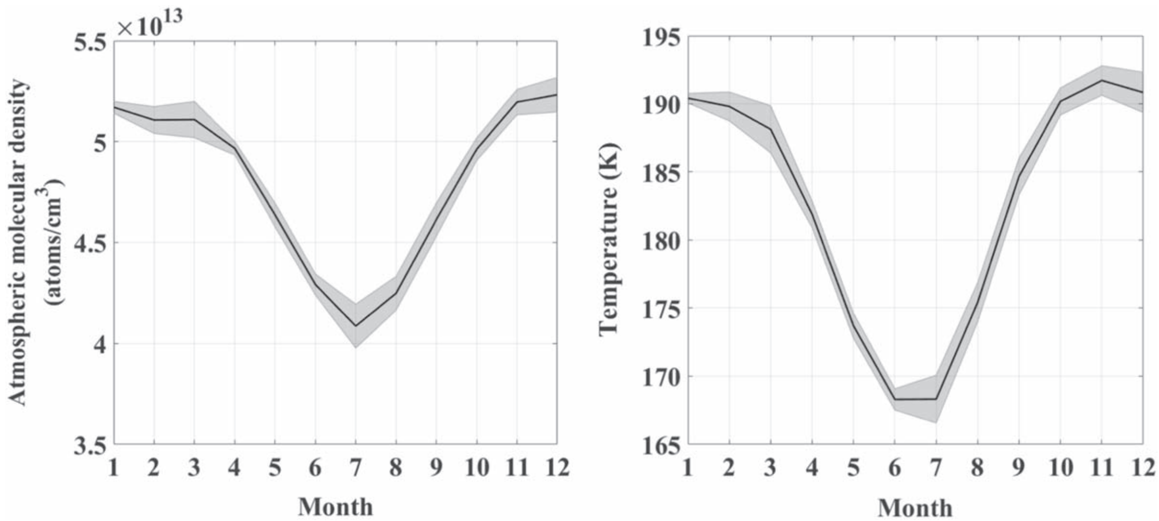

Figure 4. Nightly molecular density (left) and atmospheric temperature (right) from MSIS-90 model. *X* axes for both plots are months from January to December. Solid lines are the mean value of decade's data from 2009 to 2019 for each month at Changchun. Shaded areas represent the variation of standard deviation for each month.

sodium guide star laser to predict its on sky performance and provide guidance for its optimization. The simulation is a Monte Carlo simulation based on rate equation. During the simulated time period (for example 1 s), the state of each atom under the influence of laser light field as well as different physics such as geomagnetic field influence, light pressure, D2B repumping are being tracked every 0.2 ns. We do this process for about 900 thousands times which is sufficient for the result of the Monte Carlo simulation to converge and calculate the mean value of coupling efficiency as representative for each laser power density. And we can get the coupling efficiency versus power density carve. Comparison with field test results have been published in Jin et al. (2014, 2015), Otarola et al. (2016), Feng et al. (2016). These comparisons showed good agreement between the tool's simulated on-sky performance with actual field test measurements. In this paper, Changchun is chosen as the simulation site to facilitate the comparison with the field test results in the future.

3.1. Environment Related Parameters

The on-sky performance of the laser will also be affected by various environmental factors. According to previous texts (Kibblewhite 2000, 2008; Holzlöhner et al. 2012), the following four aspects play major roles from environmental perspectives,

1. Temperature and atmospheric molecular density.
2. Sodium layer column density and mean height.
3. Geomagnetic field on location.
4. Atmospheric seeing and transparency.

Density of large molecules in the atmosphere and temperature will affect the collision probability of sodium atoms with these molecules in the mesosphere (Kibblewhite 2000, 2008). These values could vary from months to months with a noticeable amount. Here, we used MSISE-90 model (https://ccmc.gsfc.nasa.gov/modelweb/models/msis_vitmo.php) to obtain daily night median data for these two parameters from 2009 to 2019 at an altitude of 92 km at Changchun. Figure 4 shows its monthly statistics. From this figure, one could observe that both the density and temperature had a dip in the summer time . The maximum percentages of standard deviation to mean value are less than 1.04%/2.66% for temperatures and densities, respectively, which will not cause noticeable difference to the final simulation result. Therefore, in the simulation, we used decadal monthly mean values for density of atmospheric molecule and atmospheric temperature.

The number of sodium atoms in the mesosphere directly dictates how many atoms will interact with the projected sodium laser. The column density of sodium atoms and the mean height of the sodium layer on site in zenith direction could vary dramatically from site to site, and time to time. Geo-scientist and astronomers both have studied their dynamics extensively (Fussen et al. 2004, 2010; Fan et al. 2007; Langowski et al. 2017). In general, the long term variation of sodium column density varies with the latitude of the site and the time of year of the observation which agrees quite well with long term observations of sodium layer with remote sensing satellites such as Global Ozone Monitoring by GOMOS (Fussen et al. 2004), SCIMACHY and OSIRIS (Langowski et al. 2017). Based on GOMOS data, Fussen et al. (2010) proposd an empirical Equation (1) which could be used for calculating sodium column density.

$$
\begin{aligned}
N(m, \phi)[\mathrm{cm}^{-2}] &= t_0 + t_1\cos(\frac{2\pi}{12}m + t_2)\\
&+ t_3(\phi + \frac{\pi}{2})(\phi - \frac{\pi}{2})\cos(\frac{2\pi}{6}m + t_4)\\
t_{i\leqslant 1} &= f_i(a_0 + a_1\phi + a_2\phi^2 + a_3\phi^3)\\
t_0 &= 3.28 \times 10^9. \qquad (1)
\end{aligned}
$$

Table 2
Parameters for Equation (1)

i	f_i	a_0	a_1	a_2	a_3
1	1×10^9	0.1282	1.549	0.1780	0.03511
2	1	0.4017	0.8216	−0.1282	−0.2980
3	1×10^9	−0.2630	0.1121	0.6355	−0.3566
4	1	−1.5635	−3.0526	1.3802	1.7637

In the above equation, N represents sodium atom's column density for a certain month m (0–11 represents January to December) at a certain latitude ϕ (radians). Other parameters in Equation (1) are listed in Table 2. This formula considers a constant component t_0, a yearly cycle and a semi-annual cycle. The annual cycle is most pronounced in the polar region, and its phase and amplitude are determined by the parameters t_1 and t_2. The semi-annual cycle, whose amplitude and phase are determined by the parameters t_3 and t_4, is most pronounced in the equatorial region. The different t_i are third-order polynomials in latitude ϕ (Fussen et al. 2010). According to this model, the variations of sodium column density from January to December at Changchun are shown in Figure 5. It can be seen from this figure that the sodium column density is lower in summer and higher in winter, which is similar with the variation of atmospheric molecule and temperature. In Changchun, the annual highest sodium column density is 4.65×10^{13} (atoms m^{-2}) in December and the annual lowest column density is 1.95×10^{13} (atoms m^{-2}) in summer.

Because the back-scatter emission of mesospheric sodium atoms is influenced significantly by its interaction with the geomagnetic field (Moussaoui et al. 2008, 2009), so it is necessary to take geomagnetic fields into consideration. Besides, when the telescope is tracking its object, the angle between the laser and the geomagnetic vector would gradually change, the impact of this behavior on the LGS's brightness variation also needs to be evaluated. In our simulation, one of our main purpose is to present the performance of the macro–micro pulse laser that could be easily compared with field test, therefore, except for studying the coupling efficiency in different laser projecting directions, all the simulation results are for the zenith direction which is much easier to be conducted in field test. The direction and intensity information for the geomagnetic field vector at the mesosphere's altitude at Changchun (see Table 3) are obtained from the World Magnetic Model (WMM) by the United States' National Geospatial-Intelligence Agency (NGA) (https://ngdc.noaa.gov/geomag/WMM/DoDWMM.shtml).

We used 85% for atmospheric transparency in V band in our simulation for all cases.

4. Results

In this section, we will present the predicted performance of the macro–micro pulse laser based on our simulation. Except the last subsection comparing coupling efficiencies for linear and circular polarization, polarization is defined as circular for all other simulation because of its much higher efficiency in pumping sodium atom which will lead to higher coupling efficiency of the laser.

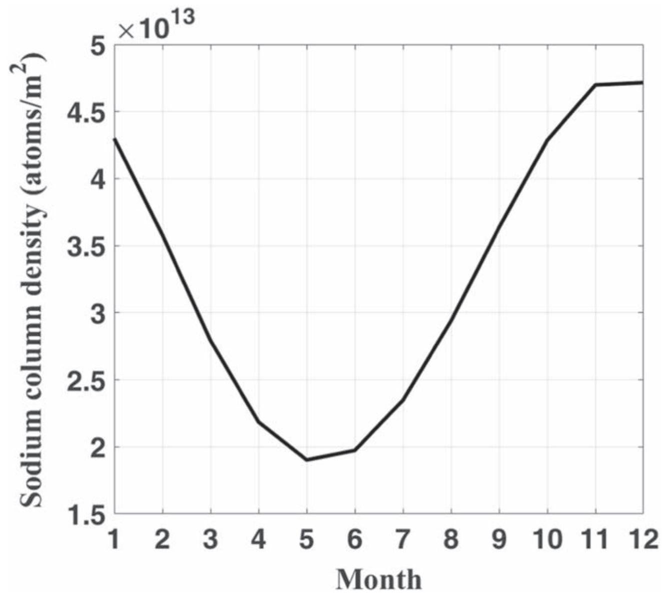

Figure 5. General trend of sodium column density variation against months based on Fussen's empirical model.

Table 3
Location of Changchun, its Geomagnetic Vectors' Intensity and Directions

Site	Longitude	Latitude	Total Intensity (nanotesla)	decl. (degree)	Inclination (degree)
Chang Chun	E 125.3°	N 43.9°	5.22×10^4	−9.55	61.70

4.1. Coupling Efficiency Variation with Different Projected Power Densities in Zenith Direction

In the simulation, the range of power density projected on to the sky at 90 km altitude is from 0.01 to 1000 W m^{-2}. All other parameters, except for power density, are the same. The direction of the laser projected is assumed to be in the zenith direction. The coupling efficiency of CIOMP laser at Changchun varies with the power density, as shown in Figure 6. The solid curve represents the mean value of the Monte Carlo simulation results while the shaded parts show the range of these results. The shaded part is wider for lower power density because in this region the probability for a sodium atom to interact with laser is also lower, a tiny number of events happening will have a large impact on the result in this region. Beside this, it can be seen from the figure that coupling efficiency of the laser increases first and then decreases with power density for Changchun. The maximum coupling

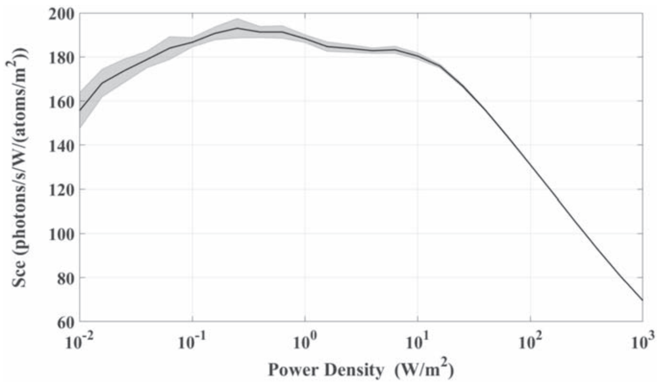

Figure 6. Coupling efficiency against projected power density on the sky (90 km) in zenith direction for Changchun. The solid curve represents the mean value of the Monte Carlo simulation results, while shaded area are the range of these results for a specific power density.

efficiency is 193 (photons s^{-1} W^{-1}/(atoms m^{-2})) at 0.25 W m^{-2} in Changchun.

4.2. Coupling Efficiency Variation with Direction of the Laser

For a typical astronomical observation, the telescope will have to change its direction to track the observation target. It is therefore necessary that the laser guide star should also be moving with the the observation target for the AO system. However, as mentioned, coupling efficiency will also change with laser emission direction because of the influence of the geomagnetic field. Therefore, for a specific site, the coupling efficiency across the whole sky has a corresponding distribution. Here we investigated the change of coupling efficiency with different elevation and azimuth angle for the laser emission direction when the power ratio for D2b re-pumping is 12%. The results for Changchun are shown in Figure 7. In this figure, the x-axis represents the azimuth angle, where 0° is for the north and 90° is for the east with a 10° increment. The y-axis represents the change of altitude angle, from 0° for the horizontal direction to 90° in the zenith direction with a 10° increment. The characteristic of the coupling efficiency distribution pattern in the sky can be summarized as follows: (1) For Changchun station, there are favorable launching directions which is related to the geomagnetic field vectors and the location of the sites. These favorable directions are quite close due to the current relatively coarse increment for the elevation angle, with an altitude angle of ~60° and an azimuth angle of ~180°. (2) Coupling efficiency distribution will be peaked at these favorable directions and will degrade noticeably around these directions, thus creating a "blob" shaped pattern. The maximum and minimum coupling efficiencies for Changchun are expected to be 352.4/94.2 photons s^{-1} W^{-1}/(atoms m^{-2}).

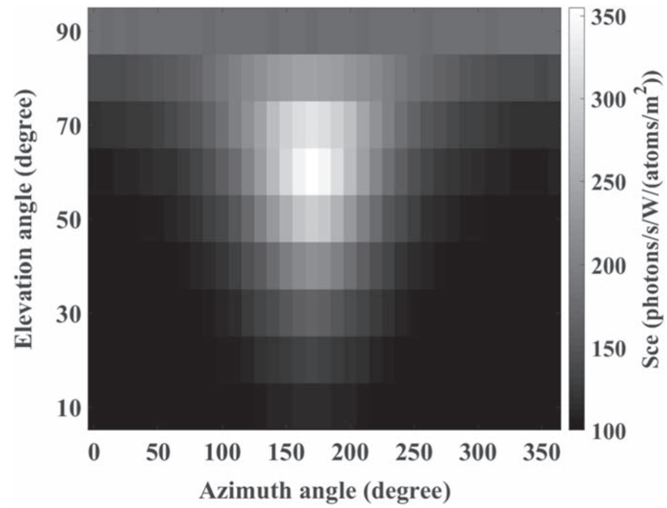

Figure 7. Coupling efficiency distribution across the sky for Changchun. X-axis is for azimuth angle. Y-axis is for elevation angle.

4.3. Coupling Efficiency Variation with Different Sodium D2b Line Re-pumping Factor

The center wavelength of the sodium laser is locked at sodium D2a line and the linewidth of the laser is only 0.5 GHz. Therefore, only the sodium atoms in the F2 ground state could be excited. However, various reasons could cause the sodium atoms to be pumped and later decayed to F1 rather than F2 ground state. This is down-pumping effect will lead to an increase of the number of sodium atoms in F1 ground state, which will then have a negative impact on photon return numbers. This situation can be improved largely by the method of D2b re-pumping (Rochester et al. 2012; Jin et al. 2015), which use a fraction of power from laser, shifted to the D2b line in order to pump sodium atoms idling in the F1 ground state. However, it's important to quantitatively balance between the percentage of power used for D2a pumping and D2b re-pumping.

Figure 8 shows the coupling efficiency of CIOMP Laser varied with different percentage of power used for D2b re-pumping in zenith direction for Changchun. As shown in the figure, when no power is used for D2b re-pumping, the coupling efficiency reaches maximum when the power density is still quite low, at about 0.1 W m^{-2} and then it will drop rapidly with the increase of power density. However, when D2b re-pumping is enabled, even if only a tiny fraction of power is used for D2b-repumping (~5%), the fast decreasing trend of coupling efficiency of the previous case will be improved. When power density is lower than ~ 0.4 W m^{-2}, the re-pumping method can not improve the coupling efficiency comparing with no D2b case. In this range, the coupling efficiency will be lower with an increasing fraction of D2b re-pumping power. Once the power density is greater than ~ 0.4 W m^{-2}, coupling efficiency will improve with an increasing of the D2b re-pumping ratio up until 30%. From the curves shown in this figure, the best power ratio for D2b is ~ 15%.

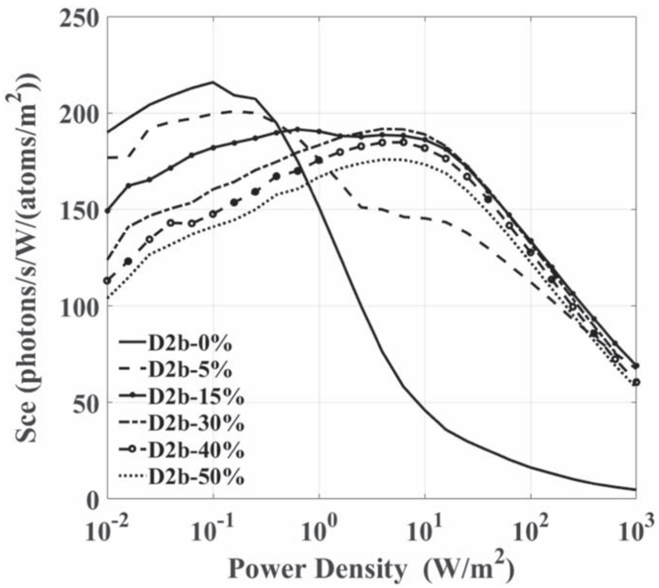

Figure 8. Coupling efficiency against projected power density in zenith direction for Changchun. Different curves represent different power ratio for D2b re-pumping from 0% to 50%.

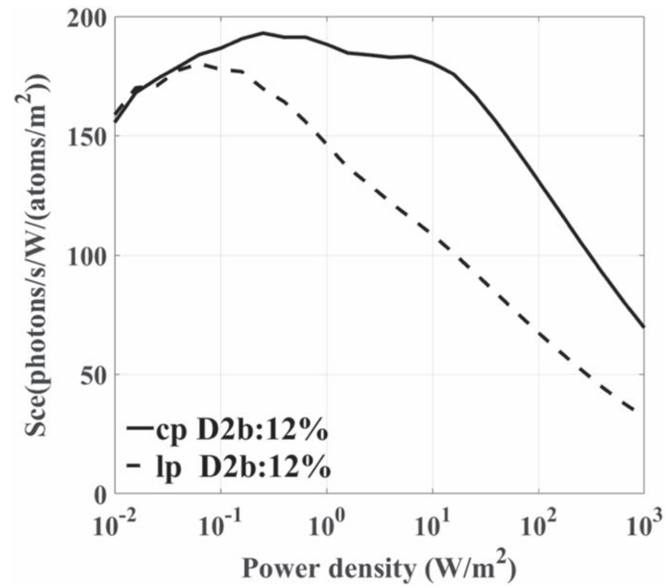

Figure 9. Linear polarization vs. circular polarization. 12% of total power is used for D2b re-pumping.

4.4. Coupling Efficiency Variation for Circular Polarization and Linear Polarization

When sodium atom is pumped to higher level by circularly polarized light or linearly polarized light, the transition selection rules are different. This leads to different photon return efficiency for linearly polarized light and circularly polarized light. The simulation results of coupling efficiency with different polarizations in Changchun are shown in Figure 9. In this picture, the solid line represents the result of circular polarization and the dotted line is for linear polarization. It can be seen from the figure that the coupling efficiency of circularly polarized light is always higher than linearly polarized light as reported in Milonni et al. (1998), Ge et al. (1998), Rabien et al. (1999), Drummond et al. (2004).

5. Discussion

In this paper, we have studied the performance of a 20W class macro–micro pulsed sodium laser in generating sodium laser guide star at one future astronomical site in Changchun, China. The predicted highest coupling efficiency for Changchun is 352.4 photons $\mathrm{s^{-1}\,W^{-1}/(atoms\,m^{-2})}$ with a D2b re-pumping ratio of 12% pointing at altitude angle of $\sim 60^\circ$ and an azimuth angle of $\sim 180^\circ$. Different projecting direction of the laser would cause a maximum of 73.27% drop of coupling efficiency across the whole sky. The D2b re-pumping technique that was previously previously proven by simulations and field tests of CW and QCW pulsed lasers is also shown to be effective when the projected power density is above $\sim 0.4\ \mathrm{W\,m^{-2}}$. The overall best power ratio for D2b re-pumping across the whole power density range is $\sim$15%. We believe this study would provide valuable performance estimation for the fabrication of the 20W macro–micro pulse laser, which would enrich the choice of sodium lasers for astronomical purpose. And in the future, we will compare the simulation and field test results in Changchun to verify the accuracy of the simulation.

The research is partly supported by the Operation, Maintenance and Upgrading Fund for Astronomical Telescopes and Facility Instruments, budgeted from the Ministry of Finance of China (MOF) and administrated by the Chinese Academy of Sciences (CAS).

References

Bian, Q., Bo, Y., Zuo, J. W., et al. 2016a, OptL, 41, 1732
Bian, Q., Bo, Y., Zuo, J. W., et al. 2020, OptL, 45, 1818
Bian, Q., Zong, Q. S., Chang, J. Q., et al. 2017, IPTL, 29, 2095
Bian, Q., Zuo, J. W., Guo, C., et al. 2016b, LaPhy, 26, 095005
Bradley, L. C. 1992, JOSAB, 9, 1931
Calia, D. B., Feng, Y., Hackenberg, W., et al. 2010, the ESO Messenger, 139, 12, www.eso.org/sci/publications/messenger/archive/no.139-mar10/messenger-no139-12-19.pdf
Calia, D. B., Hackenberg, W., Holzlöhner, R., et al. 2014, AdOT, 3, 345
Chin, J. C. Y., Wizinowich, P., Wetherell, E., et al. 2016, Proc. SPIE, 9909, 99090S
Drummond, J., Telle, J., Denman, C., et al. 2004, PASP, 116, 278
Ellerbroek, B., & Andersen, D. 2008, Proc. SPIE, 7015, 70155W
Fan, Z. Y., Plane, J. M. C., Gumbel, J., et al. 2007, ACPD, 7, 5413
Feng, L., Kibblewhite, E., Jin, K., et al. 2015, Proc. SPIE, 9678, 96781B
Feng, L., Shen, Z. X., Xue, S. J., et al. 2016, RAA, 16, 144
Fussen, D., Vanhellemont, Tétard, C., et al. 2010, ACP, 10, 9225
Fussen, D., Vanhellemont, F., Bingen, C., et al. 2004, GeoRL, 31, L24110
Ge, J., Jacobsen, B. P., Angel, J. R. P., et al. 1998, Proc. SPIE, 3353, 242

Hardy, J. W. 1998, Adaptive Optics for Astronomical Telescopes (New York: Oxford Univ. Press)

Holzlöhner, R., Rochester, S. M., Calia, D. B., et al. 2012, Proc. SPIE, 8447, 84470H

Jeys, T. H. 1991, MIT Lincoln Laboratory Journal, 4, 133, https://archive.ll.mit.edu/publications/journal/pdf/vol04_no2/4.2.3.mesosphericlaserbeacon.pdf

Jin, K., Wei, K., Feng, L., et al. 2015, PASP, 127, 749

Jin, K., Wei, K., Xie, S., et al. 2014, Proc. SPIE, 9148, 91483L

Kibblewhite, E. J. 2000, in Laser Guide Star Adaptive Optics for Astronomy, ed. N. Ageorges & C. Dainty (Dordrecht: Kluwer Academic), 51

Kibblewhite, E. J. 2008, Proc. SPIE, 7015, 70150M

Kibblewhite, E. J., Shi, F., Bonaccini, D., et al. 1998, Proc. SPIE, 3353, 300

Langowski, M. P., Savigny, C., Burrows, J. P., et al. 2017, AMT, 10, 2989

Max, C. E., Avicola, K., Brase, J. M., et al. 1994, JOSAA, 11, 813

Milonni, P. W., Fugate, R. Q., & Telle, J. M. 1998, JOSAA, 15, 217

Moussaoui, N., Holzlöhner, R., Hackenberg, W., et al. 2008, Proc. SPIE, 7015, 70152W

Moussaoui, N., Holzlöhner, R., Hackenberg, W., et al. 2009, A&A, 501, 793

Otarola, A., Hickson, P., Gagne, R., et al. 2016, JAI, 5, 1

Rabien, S., Davies, R. I., Hackenberg, W. K. P., et al. 1999, Proc. SPIE, 3762, 368

Rochester, S. M., Otarola, A., Boyer, C., et al. 2012, JOSAB, 29, 2176

Telle, J. M., Milonni, P. W., & Hillman, P. D. 1998, Proc SPIE, 3264, 37

Wang, P. Y., Xie, S. Y., Bo, Y., et al. 2014, ChPhB, 23, 904208

Xu, C., Zuo, J. W., Bian, Q., et al. 2017, ChPhL, 34, 074203